THE ASTROPHYSICAL JOURNAL, 394:459–471, 1992 August 1

ELECTROMAGNETICALLY DRIVEN RELATIVISTIC JETS: A CLASS OF SELF-SIMILAR SOLUTIONS

ZHI-YUN LI
Joint Institute for Laboratory Astrophysics, University of Colorado and National Institute of Standards and Technology, Boulder, CO 80309-0440

TZIHONG CHIUEH
Institute of Physics and Astronomy, National Central University, Chung-Li, Taiwan

AND

MITCHELL C. BEGELMAN[1,2]
Joint Institute for Laboratory Astrophysics, University of Colorado and National Institute of Standards and Technology, Boulder, CO 80309-0440
Received 1991 September 23; accepted 1992 January 6

ABSTRACT

We have constructed a class of self-similar solutions for relativistic winds driven by rotating magnetic fields. These winds are collimated to cylindrical jet flows of finite radii and may attain supermagnetosonic speeds with high Lorentz factors. Most of the flow acceleration results from the "magnetic nozzle" effect and occurs beyond the fast magnetosonic point, which is typically located a few light cylinder radii from the rotation axis. Approximate equipartition between the electromagnetic and flow kinetic energies is generally achieved for these jets, in contrast to the radial wind case in which the flow is magnetically dominated at all radii.

Subject headings: galaxies: jets — MHD — pulsars: general — quasars: general

1. INTRODUCTION

Although the speeds of jets associated with active galactic nuclei (AGNs) are not easy to obtain directly, they are believed to cover a wide range, from a few hundred kilometers per second to nearly the speed of light (Begelman, Blandford, & Rees 1984). The superluminal motion observed in some VLBI jets suggests that these collimated outflows may be moving relativistically, with a Lorentz factor ranging from about 2 to 20. For an electromagnetically driven flow, a relativistic velocity can be achieved, in principle, through a combination of the so-called magnetic sling, magnetic pinch, and magnetic nozzle effects. The plasma parcels that are tied to rotating open magnetic field lines are slung out well beyond the light cylinder centrifugally, thereby obtaining a high speed. In the meantime, the backward twisting of magnetic field lines builds up the toroidal field component which serves to collimate the outflow, and finally the compressed toroidal field can release its pressure by transferring more magnetic energy to the plasma flow, thus yielding further acceleration (Camenzind 1989).

The best studied relativistic winds operating under this mechanism are models for pulsar winds (Michel 1969; Goldreich & Julian 1970; Kennel, Fujimura, & Okamoto 1983). Unfortunately, most workers have assumed that the wind has a radial geometry, which satisfies force balance across flux surfaces only on the equatorial plane. A radial wind can be shown to be a singularly inefficient case for flow acceleration, in which the magnetic pressure force, the main accelerating force at large distances when thermal pressure is negligible, is almost exactly counterbalanced by the magnetic tension force, so that the entire flow remains submagnetosonic (Michel 1969). An arbitrarily small thermal pressure can drive a radial flow through the fast magnetosonic point but yields little additional acceleration (Kennel et al. 1983). However, supermagnetosonic speed *and* significant acceleration can be achieved, even for a cold wind, if the outflow becomes collimated (Blandford & Payne 1982, hereafter BP; Sakurai 1985; Camenzind 1987; Li & Begelman 1992). By examining the general equations for cold relativistic MHD flows, Chiueh, Li, & Begelman (1991) were able to show that the flux surfaces must become collimated toward the rotation axis under rather general conditions. In a collimated flow, the conversion of magnetic energy to kinetic energy should be much more efficient than in a radial wind.

In this paper we will demonstrate how an MHD wind can achieve both highly relativistic speeds and collimated flow, by constructing a wind solution from its source to infinity. To make this problem tractable, we will study cold flows which are self-similar in radius. The magnetic field configuration is determined self-consistently from the cross-field force balance equation, together with other flow properties (Lovelace et al. 1986). The self-similar approach has been undertaken by BP for nonrelativistic flows. Being relativistic, the flow in our problem possesses a natural length scale, the light cylinder radius, which is absent in the nonrelativistic theory. This turns out to impose a greater restriction on the class of self-similar flows than was found by BP.

Our models illustrate explicitly how the poleward bending of flux surfaces causes the fast magnetosonic point to move inward from infinity to a few light cylinder radii from the axis, in contrast to the radial wind case. While the fraction of the magnetic energy converted into plasma kinetic energy is still small at the fast point—not much different from that in the case of Michel's minimum torque solution—the "magnetic nozzle" effect continues to convert magnetic energy into plasma kinetic energy beyond the fast point until the two are comparable. This eventual approximate equipartition in a relativistic magnetized wind has been pointed out by Camenzind (1989) on the basis of numerical models (Camenzind 1987).

The plane of this paper is as follows: in § 2, we present the formulation of the problem, including a brief derivation of the

[1] Also at Department of Astrophysical, Planetary and Atmospheric Sciences, University of Colorado, Boulder.
[2] Alfred P. Sloan Foundation Research Fellow.

relativistic MHD wind equations and their self-similar forms. These equations are then solved numerically in § 3. Finally, we summarize our results and discuss their implications in § 4.

2. RELATIVISTIC SELF-SIMILAR MHD WIND

2.1. *Basic Equations*

Relativistic MHD winds have been studied previously by several authors, either with the radial wind assumption (Michel 1969; Goldreich & Julian 1970; Okamoto 1978; Phinney 1983; Kennel et al. 1983) or with full consideration of cross-field force balance (Camenzind 1986, 1987). An axisymmetric stationary flow along a flux tube is specified by four constants of motion. We shall first briefly outline the derivation of these constants of motion, and then write down the cross-field force balance equation in a form suitable for later self-similar treatment. A standard cylindrical coordinate system (R, ϕ, Z) is adopted throughout the paper, with Z measuring the distance along the rotation axis.

2.1.1. *Condition of Flux-Freezing*

Assume the plasma to be a perfect conductor, where the equation of flux-freezing $\nabla \times (\boldsymbol{V} \times \boldsymbol{B}/\gamma) = 0$ holds and implies

$$\frac{V_\phi - \gamma R\Omega(R, Z)}{V_p} = \frac{B_\phi}{B_p}$$

or, equivalently,

$$\boldsymbol{V} = \gamma R\Omega(R, Z)\hat{\phi} + \frac{k(R, Z)}{\rho}\boldsymbol{B}\,, \tag{2.1}$$

where $\boldsymbol{V}$ is the spatial part of the 4-velocity, γ is the Lorentz factor, $\hat{\phi}$ is the azimuthal unit vector, ρ is the proper plasma density, and the subscripts "p" and "ϕ" stand for poloidal and toroidal, respectively. The quantity $\Omega(R, Z)$, the angular velocity of a field line, is a constant on each flux surface, since a moving field line spans a flux surface. The quantity $k(R, Z)$ is the ratio of the mass flux to the magnetic flux and can also be shown to be a constant from the continuity equation (Chiueh et al. 1991).

If we label different flux surfaces by a poloidal flux function $\psi(R, Z)$ defined from

$$\boldsymbol{B}_p = \frac{1}{R}\nabla\psi \times \hat{\phi}\,, \tag{2.2}$$

then we have $\Omega(R, Z) = \Omega(\psi)$ and $k(R, Z) = k(\psi)$.

2.1.2. *Momentum Equation*

For a stationary flow, the special relativistic momentum equation (Goldreich & Julian 1970) is

$$\rho\boldsymbol{V}\cdot\nabla(\xi\boldsymbol{V}) = \rho_e\boldsymbol{E} + \frac{\boldsymbol{j}\times\boldsymbol{B}}{c} - \nabla P + \gamma\rho\nabla\left[\xi\gamma\frac{GM_*}{(R^2 + Z^2)^{1/2}}\right] \tag{2.3}$$

where $\xi \equiv 1 + \int dP/\rho c^2$ is the specific enthalpy, ρ and P are the proper density and proper pressure, respectively; M_* is the mass of the central star or black hole; and ρ_e is the charge density in the laboratory frame. The presence of an electric force in the MHD description is a result of relativistic effects. The quantities $\boldsymbol{E}$ and ρ_e are determined from

$$\boldsymbol{E} = -\frac{\boldsymbol{V}\times\boldsymbol{B}}{c\gamma} = -\frac{R\Omega\hat{\phi}\times\boldsymbol{B}_p}{c} = -\frac{\Omega}{c}\nabla\psi$$

and

$$\rho_e = \frac{\nabla\cdot\boldsymbol{E}}{4\pi} = -\frac{1}{4\pi c}\nabla\cdot(\Omega\nabla\psi)\,,$$

which are combined to give the electric force

$$\rho_e\boldsymbol{E} = \frac{\Omega}{4\pi c^2}\nabla\cdot(\Omega\nabla\psi)\nabla\psi\,. \tag{2.4}$$

Since the electric force is in the cross-field direction, it does not change either the energy or angular momentum along a flux surface. However, the electric force turns out to be crucial for maintaining the force balance between different flux surfaces.

2.1.3. *Energy and Angular Momentum Equations*

The conserved specific energy is obtained by taking the dot product of the momentum equation (2.3) with $\xi\boldsymbol{V}/\rho$:

$$e(\psi) = \xi\gamma c_*^2 - \frac{R\Omega B_\phi}{4\pi k}\,, \tag{2.5}$$

where

$$c_*^2 \equiv c^2 - \frac{GM_*}{(R^2 + Z^2)^{1/2}}\,.$$

The conserved specific angular momentum is obtained by taking the azimuthal component of equation (2.3):

$$l(\psi) = R\left[\xi V_\phi - \frac{B_\phi}{4\pi k}\right] = R\left[\left(\frac{\xi k}{\rho} - \frac{1}{4\pi k}\right)B_\phi + \xi\gamma R\Omega\right]. \tag{2.6}$$

Equations (2.5) and (2.6) can be used to express $\xi\gamma$ and B_ϕ in terms of e and l:

$$\xi\gamma = \frac{e}{c_*^2} - \frac{(1 - \Omega e R^2/lc_*^2)l\Omega/c_*^2}{1 - 4\pi k^2\xi/\rho - R^2\Omega^2/c_*^2} \tag{2.7}$$

and

$$B_\phi = -\frac{4\pi lk}{R}\frac{(1 - \Omega e R^2/lc_*^2)}{1 - 4\pi k^2\xi/\rho - R^2\Omega^2/c_*^2}. \tag{2.8}$$

With the help of the flux-freezing condition, we can rewrite the identity $\gamma^2 = 1 + V_p^2/c^2 + V_\phi^2/c^2$ using equations (2.7) and (2.8):

$$\frac{1}{\xi^2}\left[\frac{e}{c_*^2} - \frac{l\Omega/c_*^2(1 - R^2\Omega e/lc_*^2}{1 - 4\pi k^2\xi/\rho - R^2\Omega^2/c_*^2}\right]^2 = 1 + \left(\frac{k\xi B_p}{\rho c}\right)^2 + \left(\frac{l}{\xi Rc}\right)^2\left[1 - \frac{1 - R^2\Omega e/lc_*^2}{1 - 4\pi k^2\xi/\rho - R^2\Omega^2/c_*^2}\right]^2. \tag{2.9}$$

Because ξ is a function of ρ, equation (2.9) relates ρ to B_p along a flux surface, and since $V_p = kB_p/\rho$ is a function of B_p only, the acceleration of the flow can be determined immediately if the field geometry is known. We shall hereafter refer to equation (2.9) (and its self-similar version, eq. [2.19] below) as the energy equation.

2.1.4. *Cross-Field Force Balance Equation*

To obtain the cross-field force balance equation, we project equation (2.3) onto the unit vector $\hat{c} \equiv \boldsymbol{B}_p/B_p \times \hat{\phi}$, which is in the cross-field direction pointing towards the rotation axis. The result is

$$\kappa B_p^2\left(1 - \frac{4\pi k^2\xi}{\rho} - \frac{\Omega^2R^2}{c^2}\right) - \hat{c}\cdot\left\{\left(1 - \frac{\Omega^2R^2}{c^2}\right)\nabla\frac{B_p^2}{2} + \nabla\frac{B_\phi^2}{2} + 4\pi\gamma\rho\nabla[\xi\gamma(c_*^2 - c^2)] + 4\pi\rho c^2\nabla\xi\right\}$$
$$= \frac{B_p R\Omega}{c^2}\nabla\psi\cdot\nabla\boldsymbol{\Omega} + \frac{2B_p\Omega^2}{c^2}\nabla\psi\cdot\nabla R - \left(\frac{4\pi\rho}{R}V_\phi^2 - \frac{B_\phi^2}{R}\right)\hat{c}\cdot\nabla R, \tag{2.10}$$

where κ is the local curvature of the poloidal field lines and $\kappa B_p^2 = \hat{c}\cdot(\boldsymbol{B}_p\cdot\nabla)\boldsymbol{B}_p$.

Using equations (2.2) and (2.9) together with the definition of κ, one can write equation (2.10) as a two-dimensional second-order partial differential equation for ψ, in which all second-order terms appear on the left-hand side (Lovelace et al. 1986). As in the nonrelativistic case (BP), this equation admits three critical points along each field line, corresponding to the slow magnetosonic, Alfvén, and fast magnetosonic wave modes (Lovelace et al. 1986). By demanding that the flow pass smoothly through these points, some arbitrary parameters at the base of the flow can be fixed. The three critical surfaces are generally so complex that no attempt has yet been made to study flows with the most general boundary conditions. All past studies involve major simplifying assumptions, and our study is no exception. We are interested in relativistic flows which are sufficiently far away from the central compact source that gravity and thermal pressure probably play a dynamically insignificant role and can be neglected, i.e., $G \to 0$ and $P \to 0$ or $\xi \to 1$. These simplifications make it possible to seek scale-free (or self-similar) flow solutions. However, because of these assumptions, processes in the wind production region near the base of the flow, where gravity and thermal pressure may be important, cannot be adequately addressed.

2.2. *Relativistic Self-similar Equations*

Dimensional analysis demands that the intrinsic lengths of the problem, R, Z and the light cylinder radius $R_L \equiv c/\Omega(\psi)$, must scale similarly on each flux surface. Extracting a common ψ dependence, we require

$$(R, Z, R_L) = \frac{c}{\Omega(\psi)}(x, y, 1), \tag{2.11}$$

where the dimensionless quantities x and y have to vary in the same way on every flux surface, i.e., have to be independent of ψ. The geometric meaning of this self-similarity is shown in Figure 1. All poloidal field lines at the points intersected by any straight line emerging from the origin have the same slope. Self-similarity also demands that $\Omega(\psi)$ scale as R^{-1}, so that the linear velocity is the same at the base of each flux tube. This condition, which can be very restrictive indeed, follows from the fully relativistic nature of our treatment, and does not occur in the model of BP. The magnetic field strengths B_ϕ and B_p must scale with ψ according to

$$(B_p, B_\phi) = \frac{\Omega^2(\psi)\psi}{c^2}(b_p, b_\phi), \tag{2.12}$$

where b_p and b_ϕ are the dimensionless field strengths. Finally, from the flux-freezing condition, one can write the velocities in the form

$$(V_p, V_\phi) = c(\sigma b_p\tau x^2, \gamma x + \sigma b_\phi\tau x^2), \tag{2.13}$$

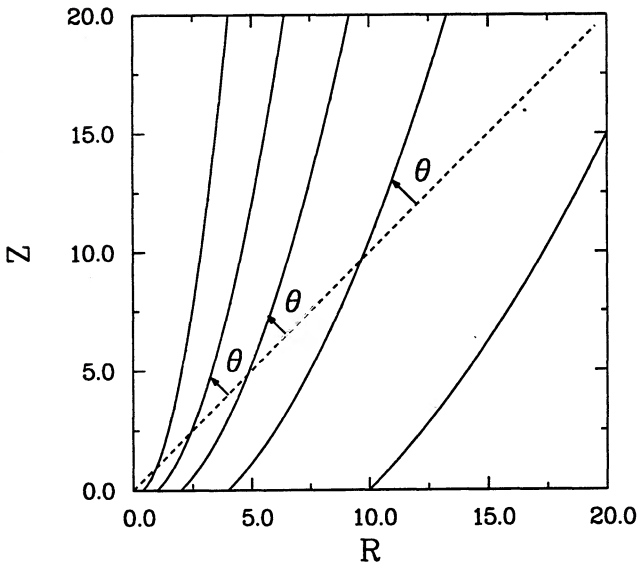

FIG. 1.—A configuration of self-similar magnetic field lines (*solid lines*) in meridional plane. The dashed line can be any straight line drawn from the origin, and the angles between the solid lines and the dashed line are all equal.

where we introduce two additional dimensionless quantities,

$$\tau \equiv \frac{4\pi k^2(\psi)}{\rho(\psi, x)x^2} \tag{2.14a}$$

and

$$\sigma \equiv \frac{\Omega^2(\psi)\psi}{4\pi c^3 k(\psi)} . \tag{2.14b}$$

In a self-similar model, both τ and σ must be flux-independent. In the radial wind literature, σ is called the magnetization parameter; its magnitude characterizes how relativistic a flow can become (Michel 1969; Goldreich & Julian 1970).

The curvature κ, b_p, and b_ϕ are readily expressed in terms of x, y, and the first two derivatives of y with respect to x ($\dot{y}$, $\ddot{y}$). We have

$$\kappa R = \frac{x\ddot{y}}{(1 + \dot{y}^{-2})^{3/2}\dot{y}^3} , \tag{2.15}$$

and the two components of $\boldsymbol{b}_p$:

$$b_r = -\frac{1}{x(x\dot{y} - y)} \frac{d(\ln\psi)}{d(\ln\Omega)} , \qquad b_z = -\frac{\dot{y}}{x(x\dot{y} - y)} \frac{d(\ln\psi)}{d(\ln\Omega)} . \tag{2.16}$$

From equation (2.8), one has

$$b_\phi = -\frac{\mu x_A^2}{\sigma x} \eta , \tag{2.17}$$

where we have defined the dimensionless specific total energy $\mu \equiv e/c^2$, the dimensionless Alfvén radius $x_A \equiv (l\Omega/e)^{1/2}$, and an auxiliary dimensionless quantity

$$\eta \equiv \frac{1 - x^2/x_A^2}{1 - (1 + \tau)x^2} , \tag{2.18}$$

to simplify expressions. Physically, η is the fraction of the angular momentum carried by the magnetic field, and at large distances ($x \gg 1$) τ is ratio of the kinetic energy flux to the Poynting flux. The variable τ is related to the magnetic field structure through the energy equation (eq. [2.9]) which, in dimensionless form, reads

$$\mu^2(1 - x_A^2\eta)^2 = 1 + (\sigma\tau b_p x^2)^2 + \frac{\mu^2 x_A^4}{x^2}(1 - \eta)^2 . \tag{2.19}$$

It is easy to verify (using eq. [2.18]) that the energy equation is a quartic in τ, and that neither dimensionless height y nor its derivative with respect to x comes in except implicitly through b_p (via eq. [2.16]). Therefore the flow acceleration as a function of x will be fixed once b_p is known.

While the above analysis holds for a rotation law $\Omega(\psi)$ of arbitrary functional form in ψ, self-similarity of the cross-field force balance equation (2.10) requires that $\Omega(\psi)$ be a power law in ψ. This requirement can be checked easily by inspection. Therefore, we let

$$\Omega = \Omega_{\rm ref}\, \chi^{-\beta}\,, \tag{2.20}$$

where $\Omega_{\rm ref}$ and β are constants and $\chi \equiv \psi/\psi_{\rm ref}$, so that

$$e(\psi) = e_{\rm ref}\,, \qquad l(\psi) = l_{\rm ref}\,\chi^{\beta}\,, \qquad k(\psi) = k_{\rm ref}\,\chi^{1-2\beta}\,, \qquad \boldsymbol{B} = (4\pi\sigma k_{\rm ref}\, c)\chi^{1-2\beta}\boldsymbol{b}\,. \tag{2.21}$$

The quantities with a subscript "ref" are evaluated along an arbitrary reference flux surface labeled $\psi_{\rm ref}$. From equation (2.16), we have

$$b_p = \frac{1}{\beta x^2}\,\frac{\sqrt{1+\dot{y}^{-2}}}{1 - y/(x\dot{y})}\,. \tag{2.22}$$

Note that if the flow becomes radial asymptotically, then one should have $\dot{y} \to y/x \to$ const as $x \to \infty$, which leads to $b_p x^2 \to \infty$. In this case, the energy equation (2.19) cannot be satisfied, which means that radial flow (i.e., flow on cones) is incompatible with the assumption of self-similarity.

Using the power-law functional form for $\Omega(\psi)$, we can simplify the cross-field equation (eq. [2.10], with $\xi \to 1$ and $c_* \to c$) by factoring out the ψ dependence in each term and casting it in the form

$$G(x, y, \dot{y}, \tau)\cdot \ddot{y} = H(x, y, \dot{y}, \tau)\,, \tag{2.23}$$

with

$$G(x, y, \dot{y}, \tau) \equiv \frac{x}{\dot{y}(1+\dot{y}^2)}\left\{\frac{1}{m_f^2}\left[1 + \left(\frac{x + y\dot{y}}{x\dot{y} - y}\right)^2\right] - 1\right\}\left(\frac{1}{m_{\rm A}^2} - 1\right) \tag{2.24}$$

and

$$\begin{aligned} H(x, y, \dot{y}, \tau) \equiv \frac{x + y\dot{y}}{\dot{y}(x\dot{y} - y)}\Bigg[&\left(2 - \frac{1}{\beta}\right)\frac{x(1+\dot{y}^2)}{x + y\dot{y}}\,\frac{1}{m_f^2}\left(\frac{1}{m_f^2} - 1\right) - \frac{1}{m_f^2}\left(\frac{1}{m_{\rm A}^2} - 1\right) - \frac{\Gamma}{\tau}\left(\frac{1}{m_f^2} - 1\right) \\ &+ \frac{2\Gamma}{\tau^2}\left(1 - \frac{1}{x_{\rm A}^2\,\eta}\right) + \frac{\Gamma^2}{\tau^3 x^2}\left(1 - \frac{1}{\eta}\right)^2\Bigg] + \frac{1}{\tau}\left(\frac{1}{m_f^2} - 1\right)\left\{2 - \frac{x(1+\dot{y}^2)}{\dot{y}(x\dot{y} - y)} + \left[\frac{1}{\tau x^2}\left(1 - \frac{1}{\eta}\right)^2 - 1\right]\Gamma\right\}\,, \end{aligned} \tag{2.25}$$

where we have defined

$$\Gamma \equiv \frac{b_\phi^2}{b_p^2 x^2}\,, \tag{2.26}$$

and the relativistic Alfvén and fast Mach numbers

$$m_{\rm A}^2 \equiv \left(\frac{V_p}{V_{\rm A}}\right)^2 = \frac{\tau x^2}{1 - x^2} \tag{2.27a}$$

and

$$m_f^2 \equiv \left(\frac{V_p}{V_f}\right)^2 = \frac{\tau b_p^2 x^2}{b_\phi^2 + b_p^2(1 - x^2)} \tag{2.27b}$$

with the Alfvénic and fast magnetosonic 4-speeds given by (Camenzind 1986)

$$V_{\rm A}^2 = \frac{B_p^2[1 - (R/R_L)^2]}{4\pi\rho}$$

and

$$V_f^2 = \frac{B_p^2[1 - (R/R_L)^2] + B_\phi^2}{4\pi\rho}\,.$$

The left-hand side of equation (2.23) derives from terms on the left-hand side of equation (2.10). It contains the entire term proportional to κ, and those parts of the $\nabla(B_p^2/2)$ and $\nabla(B_\phi^2/2)$ terms which are proportional to $\ddot{y}$. The terms of the left-hand side of equation (2.10) which are not proportional to $\ddot{y}$ are collected inside the first square brace in $H(x, y, \dot{y}, \tau)$, whereas the three terms inside the large brace in $H(x, y, \dot{y}, \tau)$ correspond to the three terms on the right-hand side of equation (2.10).

Thus far, we have reduced the cross-field equation to the second-order ordinary differential equation (2.23). This equation, together with the algebraic energy equation (2.19), will be solved numerically for the shape, $y = y(x)$, of the reference flux surface $\psi = \psi_{\rm ref}$. Before presenting the numerical integration, we analyze the critical points as well as both the near-field and asymptotic behaviors of the flow solutions.

2.3. *Critical Points*

In an MHD wind there exist three critical points, at which the poloidal flow velocity equals the propagation speed of each of the three different types of small disturbance—the slow magnetosonic wave, the Alfvén wave, and the fast magnetosonic wave (Weber & Davis 1967; Camenzind 1986). For a cold wind, the neglect of thermal pressure implies the absence of a slow magnetosonic point.

The possible singular points in the energy equation are revealed by differentiating equation (2.19) once, so that

$$\frac{d\tau}{dx} = \frac{1}{(1/m_A^2 - 1)^2(1/m_f^2 - 1)} \left[\frac{\mu^2 x_A^4}{\sigma^2 \tau^2 b_p^2 x^9} \left[\left(\frac{1}{m_A^2} - 1 \right) - \frac{1}{\tau} \left(\frac{1}{x^2} - \frac{1}{x_A^2} \right) \right] \right.$$
$$\left. \times \left\{ 2\left(1 - \frac{x^2}{x_A^2} \right) + \tau x^2 \left[\left(\frac{1}{m_A^2} - 1 \right) - \frac{1}{\tau} \left(\frac{1}{x^2} - \frac{1}{x_A^2} \right) \right] \left(\frac{1}{m_A^2} - 1 \right) \right\} + \tau \left(\frac{1}{m_A^2} - 1 \right)^3 \left[\frac{x + y\dot{y}}{(1 + \dot{y}^2)(x\dot{y} - y)} \ddot{y} - \frac{1}{x} \right] \right] . \quad (2.28)$$

The above equation is singular when the denominator vanishes while the numerator remains finite. At such a point, two root branches of $\tau(x)$ in the quartic energy equation (2.19) merge, and switch from imaginary to real or from real to imaginary. It is only at a "regular" singular point, where the denominator and the numerator vanish simultaneously, that two real root branches can cross each other and remain as real branches after crossing. The Alfvén point is such a point, since it ($m_A = 1$) always occurs automatically at $x = x_A$ from the requirement that the toroidal field strength vary continuously cross the Alfvén point (cf. eq. [2.18]). This situation also arises in a radial wind. As a result, the requirement of trans-Alfvénic flow does not impose any constraints on the flow parameters via the energy equation. What is not so obvious, however, is the fast point ($m_f = 1$) is also always a "regular" singular point of equation (2.28), so that solutions can pass through it *smoothly, without imposing any constraint.* This situation differs drastically from that of a radial wind (Goldreich & Julian 1970; Kennel et al. 1983). It is the presence of $\ddot{y}$ in equation (2.28) that makes the picture entirely different. In fact, whenever $m_f = 1$, equation (2.23) can always be so arranged as to yield an expression for $\ddot{y}$ that makes the numerator of equation (2.28) vanish simultaneously. The extra degree of freedom afforded by curvature of the flux surfaces makes this self-adjustment possible.

Analysis of the cross-field equation, equation (2.23), reveals the true singularities of the problem, at which constraints on the flow parameters must be imposed in order to obtain smooth passage of the flow. From the expression for $G(x, y, \dot{y}, \tau)$, it is apparent that the singularities of equation (2.23) occur at the Alfvén point, $m_A = 1$, and at a modified fast magnetosonic point, $m_f^2 = 1 + [(x + y\dot{y})/(x\dot{y} - y)]^2$. The former occurs quite generally in axisymmetric winds which satisfy cross-field force balance (Sakurai 1985 gives a detailed discussion for nonrelativistic flows), and a regularity condition $H(x_A, y_A, \dot{y}_A, \tau_A) = 0$ has to be imposed in order to ensure that the solution passes through it smoothly. The latter is equivalent to $m_f \sin\theta = 1$, where $\theta \equiv \sin^{-1}\{|x\dot{y} - y|/[(x^2 + y^2)(1 + \dot{y}^2)]^{1/2}\}$ is the angle between the tangent of the field line at point (x, y) and the spherical radius passing through that point (see Fig. 1). The peculiar angular modification of the critical point condition arises from the assumption of self-similarity, which imposes the constraint that all flow properties along any radial cone should be similar. A wave propagating in the flow must have the same phase at all points on the cone, and therefore can propagate only in the polar direction. In this direction, the Alfvén wave has a wave speed $V_A \sin\theta$ and the fast magnetosonic wave has a speed V_f. Since a critical point is physically a location at which the flow speed matches the wave speed in the direction of propagation, the relevant component of the flow speed to compare is therefore $V_p \sin\theta$. It immediately follows that the critical points should occur at the locations indicated above. These arguments have been given by BP, who first recognized the importance of the modified fast point.

A solution to the cross-field equation (2.23) which passes smoothly through the Alfvén point can be obtained by applying l'Hôpital's rule. Since this approach has been fully elaborated in other works, we will not dwell on it. The modified fast point, however, is something relatively new in the MHD wind literature, and therefore deserves further attention. As we show in the next section, a wide range of solutions which pass the Alfvén point may subsequently encounter the modified fast point. These solutions are distinguished by different values of the specific energy μ. Solutions are always found to be singular where they encounter the modified fast point at a finite height. The only way around this difficulty is to adjust the value of μ such that the modified fast point moves to an infinite height so as to be avoided.

2.4. *Near-Field Expansion*

Near the base of the flow, the magnetic field lines are rigid and nearly force-free. It can be shown that it is impossible for all field lines to emerge from the origin, to maintain cross-field balance and still to be self-similar. Therefore, we shall focus on situations where the field lines on a given flux surface are anchored to a thin equatorial disk ($y = 0$) at some finite radius $R_0 [= x_0 c/\Omega(\psi)$, where subscript "0" denotes quantities evaluated at base of the flow]. Immediately above the base of the flow, the poloidal velocity is taken to be zero, and the plasma is assumed to corotate with the field line. From this start-up flow condition, we find, from equation (2.19), that

$$\mu(1 - x_A^2) = \sqrt{1 - x_0^2} , \quad (2.29)$$

that is, Alfvén point is located at $x_A = [1 - (1 - x_0^2)^{1/2}/\mu]^{1/2}$, which is always inside the light cylinder. Since we have neglected gravity, there is no force to compete with the centrifugal force. Therefore, as long as the field lines have a component directing outward, parcels of plasma can always be accelerated centrifugally, regardless of the angle at which the field line is anchored to the disk (in contrast to the case considered by BP). The poloidal velocity of the parcels scales with the radial distance from the base of the flow as $(\delta x)^{1/2}$ for small $\delta x \equiv x - x_0$. Given the form of the poloidal velocity, we can expand equations (2.19) and (2.23) about $x = x_0$, $y = 0$, and $\tau = 0$ (from $u_p \equiv V_p/c = \sigma\tau b_p x^2$) to obtain the shape of the field lines and the velocity profile. We find that both the energy equation (2.19) and the cross field balance equation (2.23) are satisfied by the following expansions:

$$y = y_1 \delta x + y_2 \delta x^{3/2} + \cdots \quad (2.30a)$$

and

$$\tau = \tau_1 \delta x^{1/2} + \tau_2 \delta x + \cdots \tag{2.30b}$$

where τ_1, y_2, and τ_2 are related to the initial slope of the field line y_1 by

$$\tau_1 = \frac{1-\eta_0}{\eta_0 x_0^2}\sqrt{\frac{2\Gamma_0 x_0(1-x_0^2)}{\Gamma_0 x_0^2 + (1-x_0^2)}}$$

$$y_2 = \frac{4}{3}\frac{\Gamma_0 y_1^3(1-\eta_0)^2}{\eta_0^2 \tau_1 x_0(1-x_0^2)}\left[1 + \frac{\Gamma_0 x_0^2}{\Gamma_0 x_0^2 + (1-x_0^2)}\right]$$

$$\tau_2 = -\frac{\Gamma_0 x_0}{\Gamma_0 x_0^2 + (1-x_0^2)}\left[\frac{x_0^2 \tau_1^2}{1-x_0^2} + 2\left(1 - \frac{1}{x_A^2 \eta_0}\right) + \frac{2\tau_1(1-\eta_0)}{\eta_0 x_0^2}\right]$$

$$+ \frac{3\tau_1(1-x_0^2)y_2}{2y_1(1+y_1^2)[\Gamma_0 x_0^2 + (1-x_0^2)]}, \tag{2.31}$$

with

$$\eta_0 = \frac{1-(x_0/x_A)^2}{1-x_0^2}, \qquad \Gamma_0 = \frac{\mu^2\beta^2 x_A^4 \eta_0^2 y_1^2}{\sigma^2(1+y_1^2)}. \tag{2.32}$$

Finally, we can obtain the poloidal dimensionless 4-velocity from

$$u_p = \sigma\tau b_p x^2 = \frac{\sigma\tau_1\sqrt{1+y_1^2}}{\beta y_1}\left\{\delta x^{1/2} + \left[\frac{\tau_2}{\tau_1} - \frac{3y_2}{2y_1(1+y_1^2)}\right]\delta x + \cdots\right\}. \tag{2.33}$$

The near-field solutions can be used to initiate the numerical integration at the base of the flow. The free parameter y_1—the slope of the field line at the base—is to be fixed by requiring the solution of the force balance equation (2.23) to be regular at the Alfvén point.

2.5. *Far Field Solutions*

Asymptotic structures of hydromagnetically-driven winds have been studied by Heyvaerts & Norman (1989) in the nonrelativistic limit, and by Chiueh et al. (1991) in the relativistic limit. Asymptotic flux surfaces may converge to "cylinders" (if $R \to$ const as $Z \to \infty$), "paraboloids" (if $R/Z \to 0$ and $R \to \infty$ as $Z \to \infty$) or "cones" (if $R/Z \to$ const as $Z \to \infty$). As discussed in § 2.2, conical flux surfaces are excluded in a self-similar wind.

We first consider asymptotically paraboloidal flux surfaces. Let $[\ldots]_\infty$ denotes a quantity evaluated asymptotically. It is evident from equation (2.22) that $(b_p x^2)_\infty$ cannot vanish in a self-similar flow. In the limit of finite $(b_p x^2)_\infty$ and $R/R_L \to \infty$, the cross-field force balance equation (2.10) reduces to

$$\frac{d}{d\psi}\left(\frac{B_p R^2 \Omega}{V_p}\right)_\infty^2 = 0 \tag{2.34}$$

(Chiueh et al. 1991). Upon substituting the self-similar scalings, the above equation becomes

$$(1-\beta)\left(\frac{\psi}{\psi_{\rm ref}}\right)^{1-2\beta}\left(\frac{4\pi\sigma k_0 c^2}{\Omega_0}\right)^2\left(\frac{b_p x^2}{V_p/c}\right)_\infty^2 = 0. \tag{2.35}$$

Equation (2.35) can be satisfied only if $\beta = 1$, which corresponds to the current-carrying (Type I) paraboloids discussed by Chiueh et al. (1991).

Asymptotically current-carrying paraboloidal flux surfaces were also found by BP in their far field analysis of a nonrelativistic self-similar wind. The fast critical points for these solutions are always located at infinity. However, because of relativistic effects and the fact that our velocity scaling law ($\Omega \propto \psi^{-1}$) differs from that used by BP, the above statement is not necessarily true in our case. A numerical example to illustrate this point is given in § 3.

For current-carrying paraboloids, all of the current I is concentrated asymptotically on the rotation axis. This is because the total current $I_\infty(\psi)$ enclosed by an arbitrary flux surface ψ asymptotically is $I_\infty = (B_\phi R)_\infty c/2 = (b_\phi x)_\infty c/2 =$ const when $\beta = 1$. In our previous paper (Chiueh et al. 1991), we regarded the current-carrying paraboloids as unphysical because of the singular axial line current. We include them in this analysis for the sake of comparison with the work of BP.

Next we consider asymptotically cylindrical flux surfaces. We shall show that this type of flux surface exists only for $\beta < 1$. To do this, we find it more convenient to use $t \equiv \ln y$ as the independent variable and to treat x as the dependent variable. Equation (2.23) can then be rewritten as

$$\frac{d^2x}{dt^2} = x'\left[1 - \frac{x' N(t, x, x', \tau)}{D(t, x, x', \tau)}\right] \tag{2.36}$$

where a prime denotes the derivative with respect to t, and expressions for $N(t, x, x', \tau)$ and $D(t, x, x', \tau)$ are given in the Appendix. An

asymptotically cylindrical surface demands that $x \to x_\infty$ (finite) and $x' \to 0$ as $t \to \infty$. In this limit we obtain, to the leading order,

$$D(t, x, x', \tau) \to (x')^2 D_1(x_\infty, \tau_\infty), \qquad N(t, x, x', \tau) \to N_0(x_\infty, \tau_\infty), \tag{2.37}$$

where expressions for $D_1(x_\infty, \tau_\infty)$ and $N_0(x_\infty, \tau_\infty)$ are also given in the Appendix. It is easy to check by inspection that an asymptotically cylindrical solution cannot exist unless $N_0(x_\infty, \tau_\infty) = 0$. Otherwise $x|_{t\to\infty}$ becomes infinite.

Since $N_0(x_\infty, \tau_\infty)$ must vanish, the lowest nonvanishing term in the Taylor expansion of $N(t, x, x', \tau)$ about x_∞ is proportional to x', i.e., $N(t, x, x', \tau) \to x' N_1(x_\infty, \tau_\infty)$, so that

$$y = e^t = C_1 \Delta x^{-\alpha_1}, \tag{2.38a}$$

in the vicinity of x_∞, for small $\Delta x \equiv x_\infty - x$. The quantity C_1 is an integration constant, and the exponent

$$\alpha_1 = \left[\frac{N_1(x_\infty, \tau_\infty)}{D_1(x_\infty, \tau_\infty)} - 1\right]^{-1} \tag{2.38b}$$

has to be positive in order that $y \to \infty$ as $\Delta x \to 0$.

The condition $N_0(x_\infty, \tau_\infty) = 0$ and the energy equation (2.19) at the asymptotic cylinder radius yield two coupled algebraic equations for the two unknowns x_∞ and τ_∞, which are solved numerically given the constants x_0, σ, β, and μ. We find that physical solutions with finite, positive x_∞ are possible only for $\beta < 1$, and that $x_\infty \to \infty$ as $\beta \to 1$. Solutions with $\beta > 1$ cannot extend asymptotically to cylinders and contain unphysical infinite current densities on their axis, since the current enclosed within a radius R scales as $R^{(1-\beta)/\beta}$. When the limiting radius lies far beyond the light cylinder ($x_\infty \gg 1$) and the asymptotic flow is highly relativistic ($u_\infty \gg 1$), the energy equation (2.19) reduces to $u_\infty \cong \mu - \sigma/\beta$, which can be used to obtain τ_∞ since $u_\infty = \sigma\tau_\infty (b_p x^2)_\infty \cong \sigma\tau_\infty/\beta$ (cf. eq. [2.22]). The radius x_∞ turns out to be a monotonically increasing function of β for given σ and μ, but is insensitive to x_0 as long as x_0 is small. Physically, a smaller β means that the magnetic field is relatively stronger at a given radius according to the scaling $B \propto R^{1/\beta - 2}$, and thus it also implies better collimation. In Figure 2, we have plotted $\log_{10}(x_\infty)$ against β for $x_0 = 0.1$ and $\sigma = 5.0$, 10.0, and 50.0, assuming $\mu = 2\sigma$. The latter assumption is approximately true for critical solutions with $\sigma \gg 1$, as will be evident from § 3.3 below.

Once x_∞ and τ_∞ are known, the exponent α_1 given by equation (2.38b) is readily calculable, since $D_1(x_\infty, \tau_\infty)$ can be obtained by direct substitution and $N_1)x_\infty, \tau_\infty)$ by l'Hôpital's rule. As noted above, α_1 must be positive to ensure a valid solution.

Given σ and $\beta < 1$, we can find a radius x_∞ for every $\mu > 1$. However, solutions initiated from the base of the flow with a given value of μ are not necessarily able to approach this limiting-cylindrical radius x_∞ smoothly. In fact, as we shall show below numerically, only one "critical" solution, with a unique specific energy μ_c, can actually reach the limiting cylinder. Solutions with μ not equal to μ_c will have a turning point at some finite height and radius, where the initially transversely expanding flux surfaces will start to pinch back towards the rotational axis (see also BP). Reconvergence of the flux surfaces beyond the turning point makes $\dot{y}$ negative, and eventually the quantity $b_p x^2$ begins to decrease.

According to the energy equation (2.19), one obtains two different solution behaviors in the limits $x \gg 1, b_p x^2 \to 0$ and $\mu \gg 1$:

$$m_f^2 \cong \frac{\mu^3}{\sigma b_p x^2} \quad \text{(supermagnetosonic)} \tag{2.39a}$$

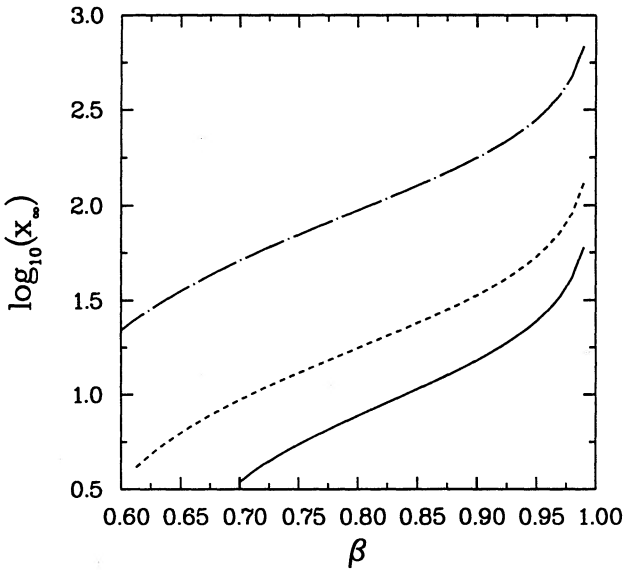

FIG. 2.—The limiting cylinder radius x_∞ is plotted as a function of the parameter β for $\sigma = 5.0$ (*solid*), 10.0 (*dashed*), and 50.0 (*chain-dotted*). We have assumed $\mu = 2\sigma$ and $x_0 = 0.1$.

or

$$m_f^2 \cong \frac{\sigma^2}{\mu^3}(b_p x^2)^2 \quad \text{(submagnetosonic)} \tag{2.39b}$$

depending on which branch the solution is on. On the supermagnetosonic branch ($m_f > 1$), the fast Mach number m_f increases as $b_p x^2$ decreases, whereas on the submagnetosonic branch ($m_f < 1$), the opposite holds. This is analogous to the hydrodynamic "nozzle" effect and is thus termed the "magnetic nozzle" effect. The solutions on the former branch have total energy $\mu < \mu_c$ where the rapid increase of m_f leads $m_f \sin\theta$ to approach unity and hence to encounter the modified fast point (§ 2.3) at some finite height, whereas the solutions on the latter branch have $\mu > \mu_c$ and apparently stop at the point at which $b_p x^2 = 0$.

3. NUMERICAL INTEGRATIONS

3.1. *Critical Cylindrical Solutions*

As pointed out in § 2.3, the relativistic Alfvén point at $x = x_A$ is a critical point of the cross-field equation (2.23), at which a regularity condition $H(x_A, y_A, \dot{y}_A, \tau_A) = 0$ has to be imposed. The Alfvén radius x_A is fixed once the flow constants x_0, σ, $\beta < 1$, and μ are given. By eliminating τ_A from the energy equation (2.19) in favor of the slope $\dot{y}_A$ and the height y_A at the Alfvén point, one can calculate $\dot{y}_A$, and thus $\ddot{y}_A$ (using l'Hôpital's rule on eq. [2.23]), for a given value of y_A. This alows for integration of equation (2.23) both inward and outward from the Alfvén point. The undetermined height y_A can be fixed by matching the inward integration from the Alfvén point onto the outward integration from the base of the flow using the near-field expansion developed in § 2.4. This process simultaneously fixes the parameter y_1, the slope of the field line at the base. Clearly, the regularity condition completely determines the inner part of the solution up to the Alfvén point and does not impose any constraint on the flow constants.

Once the smooth solution from the base of the flow to the Alfvén point is found by iteration, there is no difficulty in shooting outward from the Alfvén point, passing automatically through both the light cylinder and the conventional relativistic fast point $m_f = 1$, which is generally located at only a few light cylinder radii from the rotation axis when σ (the relativistic parameter) is comparable to or larger than unity. In practice, due to the rapid increase of y with respect to x, we change variables and switch to integrating equation (2.36) in order to obtain solutions extending to a great distance from the source.

The solutions beyond the fast point generally do not yield physically meaningful asymptotes. They fall into two categories, as mentioned towards the end of § 2.5. Both categories of solution eventually bend back toward the rotation axis as the flow travels upward, presumably because the outward inertial force becomes too weak to counteract the unbalanced magnetic pinch force. One category of solution has a smaller μ, and the flow accelerates as it gets pinched, until the modified fast point is reached. The other category has a larger μ, and the flow decelerates as it is pinched; this continues until the flow stops. Nonetheless, there exists a critical μ_c at the boundary of the two types of solution, for which the outward inertial force just balances the electromagnetic force, in such a way that the flow expands outward until it reaches a limiting radius.

Plotted in Figure 3 are the results of integrating equation (2.23) from the source $x = x_0$ to a point just outside the fast point and then switching to integration of equation (2.36) beyond. For illustrative purposes, we have chosen $\sigma = 10.0$, $\beta = 0.95$, and $x_0 = 0.1$. In these plots, different curves correspond to different choices for the total specific energy: $\mu = 21.8620$ (*dotted*), 21.8625 (*solid*), 22.2200 (*dashed*). Figure 3*a* shows the shapes of the field lines, which are nearly degenerate out to several light cylinder radii for the

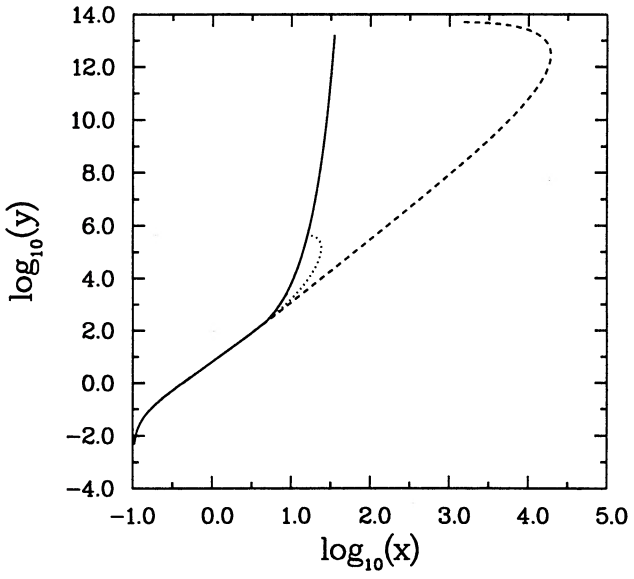

FIG. 3*a*

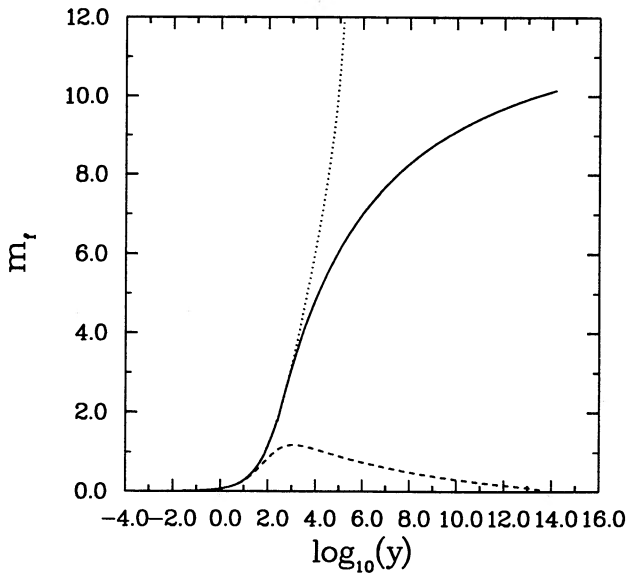

FIG. 3*b*

FIG. 3.—(*a*) Log-log plots of the magnetic field structure for three different energies: $\mu = 21.8620$ (*dotted*), 21.8625 (*solid*), and 22.2200 (*dashed*), and (*b*) their corresponding fast magnetosonic Mach numbers as function of the height.

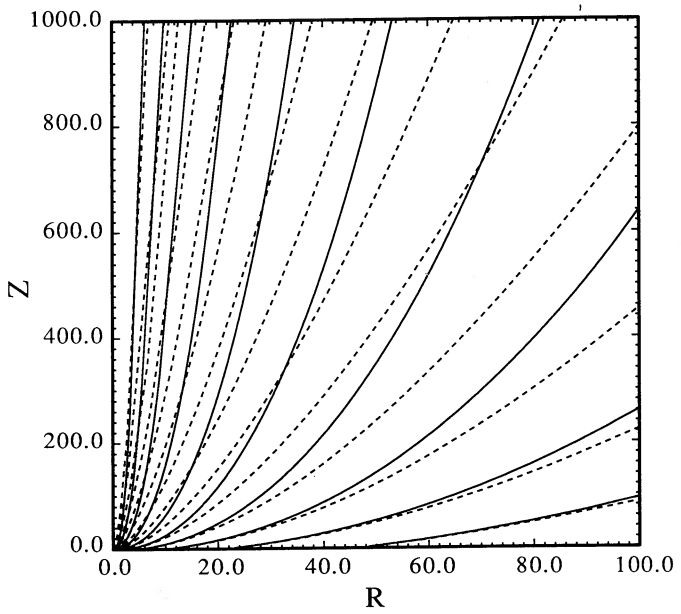

FIG. 4

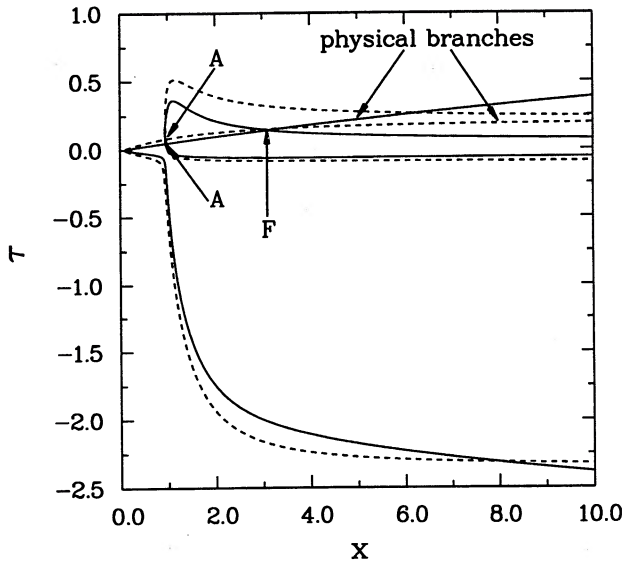

FIG. 5

FIG. 4.—The poloidal magnetic field lines (*solid*) and the lines of the poloidal current density (*dashed*), for the critical cylindrical solution in Fig. 3 (*solid*). The crossing of the two sets of lines is evident.

FIG. 5.—Solution topologies of the energy equation (2.19) for the critical solution in Fig. 3 (*solid*) and a radial wind (*dashed*) with the same magnetization parameter $\sigma = 10$. The Alfvén point (labeled A) and the fast magnetosonic point (labeled F) correspond to intersections between the "physical branch" of the solution of the equation and other solution branches.

parameters chosen. Plotted in Figure 3*b* are the fast Mach numbers as functions of the height above the equatorial plane. Clearly, the behaviors of the solutions far beyond the light cylinder are completely different for these different energies. The solution with $\mu = 21.8625 = \mu_c$ asymptotically goes to a cylinder, whereas the other two are representative of the two distinctive types of solutions with μ less than and greater than μ_c, respectively. The one with $\mu < \mu_c$ becomes singular at $m_f \sin\theta = 1$, while the one with $\mu > \mu_c$ starts to decelerate at some finite height and eventually stops, as mentioned earlier. In Figure 4 we plot, for the critical cylindrical solution ($\mu = \mu_c$), lines (*dashed*) of the poloidal current density j_p, which cross the poloidal magnetic field lines (*solid*) and are responsible for most of the flow acceleration along the flux surfaces.

To contrast the self-similar critical solution with the critical solution of a radial wind, we solve for τ from the energy equation (2.19), a quartic equation in τ. Plotted in Figure 5 are the real roots of the energy equation for the critical solution discussed above (*solid lines*), and for a radial wind (*dashed lines*, from Michel 1969) with the same σ. The physical roots in both cases are marked. Near the origin, each case has only two real roots, one of which has $\tau < 0$ and is therefore unphysical. Two additional roots appear at some point inside the Alfvén radius. One of the new roots intersects the physical root at the Alfvén point (labeled A). A second intersection between one of the new roots and the physical root occurs at the fast magnetosonic point, which is located at $x_f = 3.3$ (labeled F) for the self-similar case but which lies at infinity for the radial case (Goldreich & Julian 1970).

Most of the flow acceleration for the critical solution occurs beyond the fast critical point. If we plot the specific kinetic energy γ as a function of radius (Fig. 6), then it is evident that the specific kinetic energy at the fast point $\gamma_f = 2.87$ is close to the cube root of the total energy $\mu_c^{1/3} = 2.80$, as in the case of radial wind, while the asymptotic Lorentz factor $\gamma_\infty = 11.30$ is much larger. Thus, major acceleration indeed takes place after the fast point is passed. We find that this property is common to all critical solutions with large σ, as long as β is close to unity.

3.2. *Critical Paraboloidal Solutions*

Paraboloidal flow solutions with $\beta = 1$ have the same topologies as cylindrical solutions with $\beta < 1$. In particular, given x_0 and σ, we find that there exists one μ_c that makes the solution extend smoothly from the base of the flow to infinity. Other solutions either are terminated at the modified fast point when $\mu < \mu_c$ or slow down to zero velocity when $\mu > \mu_c$. Plotted in Figure 6 is the acceleration curve for the critical paraboloidal solution with $x_0 = 0.10$ and $\sigma = 10.0$. The fast magnetosonic point is located at a finite distance, which is different from the family of paraboloidal solutions found by BP.

3.3. *Energy Partition in the Flow*

The value of the critical energy μ_c is determined by x_0, β, and more importantly, σ. It turns out that μ_c is insensitive to x_0 as long as x_0 is small, i.e., provided the linear speed of the rotating magnetic field at the base of the flow is much less than the speed of light. Table 1 shows how μ_c, the terminal Lorentz factor γ_∞, and the limiting cylinder radius x_∞ depend on σ and β, for $x_0 = 0.1$. Several features are clear from Table 1. First, we notice that μ_c is also insensitive to the value of β; therefore the approximate relation $u_\infty \cong \mu_c - \sigma/\beta$ derived in § 2.5 implies that the larger β is the greater acceleration there will be. Second, most of the μ_c's in Table 1 are about twice as large as their corresponding σ's, except for those of small σ (the column $\sigma = 1.0$ in Table 1). Thence we deduce

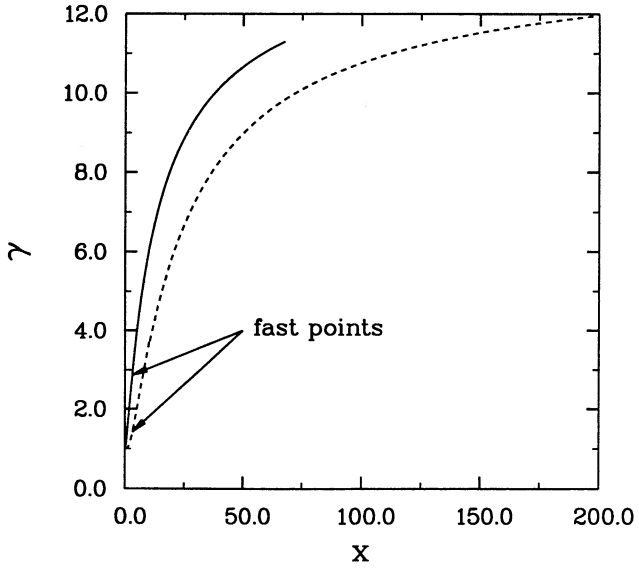

FIG. 6.—Acceleration curves of the critical cylindrical solution in Fig. 3 (*solid*) and the critical parabolic solution (*dashed*) with $\beta = 1$, $\sigma = 10$, and $x_0 = 0.1$.

from the foregoing approximation for u_∞ that, if β is close to unity, the kinetic energy approaches about half of the total energy, or equivalently, that the kinetic energy flux will come nearly into equipartition with the Poynting flux.

4. CONCLUSIONS AND DISCUSSION

We have explored a class of relativistic, hydromagnetic jet flows which exhibit self-similar scaling in radius. We find, in agreement with BP's work on self-similar nonrelativistic winds, that all such flows collimate along the rotation axis. It turns out that the asymptotic behaviors of the flow solutions are determined by the scaling of the rotation law, $\Omega \propto \psi^{-\beta}$. The flux surfaces are asymptotic to cylinders when $\beta < 1$, and become paraboloidal when $\beta = 1$. Our flows can attain highly relativistic speeds, with most of the acceleration occurring beyond the fast magnetosonic point through the "magnetic nozzle" effect.

The applicability of our solutions to realistic astrophysical systems is limited by the restrictions necessary to obtain a self-similar solution. The assumption of self-similarity demands that no length scale be present in the problem. Since a special relativistic treatment imposes a velocity scale, c, we require that all components of the velocity be the same at corresponding points of all flux surfaces. This implies that the angular velocity at the base of the flow must scale according to $\Omega \propto R^{-1}$. Thus, we are unable to treat a relativistic wind emanating from a Keplerian disk (as was treated by BP in the nonrelativistic limit), although such a wind is certainly possible in principle. We are also unable to include the effects of gravity and pressure within the self-similar framework.

Nevertheless, our solutions capture several important aspects of relativistic MHD winds which are likely to apply to non–self-similar flows as well. In particular, they exhibit the tendency toward asymptotic collimation and approximate equipartition between the kinetic energy flux and the Poynting flux of the flow. These features were found, for example, by Sakurai (1985, 1987), who constructed numerical models of nonrelativistic winds, assuming a split monopole field geometry at the flow base. The most thorough investigations so far on relativistic winds driven by rotating magnetic fields were carried out by Camenzind (1986, 1987). In his model calculations, the magnetosphere is assumed to be sparsely populated with plasma. Not only the Alfvén radius is located at the light cylinder, but also the plasma current was negligibly small so that all field lines cross the light cylinders horizontally; the flow begins to collimate only beyond the light cylinders. The finite plasma current is included in our treatment, as is evident from the fact that field lines cross the light cylinder with a finite slope. Therefore, collimation may occur even well inside the light cylinder. Another difference between Camenzind's calculations and ours is that he assumed that the fast point lies far beyond the light

TABLE 1

DEPENDENCES OF THE CRITICAL ENERGY μ_c AND THE TERMINAL FLOW LORENTZ FACTOR γ_∞ ON PARAMETERS σ AND β FOR $x_0 = 0.1$

FLOW VARIABLES	β	σ = 1	5	20	50
μ_c	0.95	3.58	11.80	41.93	102.01
	0.90	3.55	11.75	41.85	101.93
	0.80	3.51	11.68	41.74	101.76
	0.70	3.50	11.63	41.68	101.69
γ_∞	0.95	2.42	6.47	20.85	49.37
	0.90	2.32	6.12	19.60	46.36
	0.80	2.10	5.32	16.70	39.24
	0.70	1.86	4.33	13.04	30.23

cylinder in order to allow for a simple outer boundary conditions, whereas the fast point in our self-similar flows is located typically only a few light cylinder radii from the rotational axis. Common to both calculations is the fact that, at the fast point, the flow attains a Lorentz factor of order $\mu^{1/3}$ and most of the energy flux is stored in the form of Poynting flux. It is only through the so-called magnetic nozzle effect beyond the fast point that the Poynting flux continues to be converted into kinetic energy flux.

It is worth noting that neglecting the inertia of the wind plasma yields a family of force-free solutions which are confined within the light cylinder (Sulkanen & Lovelace 1990). These solutions are not simply the highly magnetized wind solutions in the high σ (i.e., low mass-loading rate) limit. The inclusion of the plasma inertia, however small it is, would remove the singularities at the light cylinder that prevent the force-free solutions from crossing. In fact, the important processes of flow acceleration, especially those occurring beyond the light cylinder, are not captured at all in force-free solutions.

To contrast our relativistic self-similar solutions with those found by BP, we first note that the scalings of flow variables at the base are different in the two cases. It is therefore not suprising that we do not necessarily recover all of their results, even in the limit of low σ (nonrelativistic). In particular, the family of asymptotically paraboloidal solutions they found always have $m_f = 1$ at infinity, whereas a similar family of solutions (with $\beta = 1$) in our case do not have such a property in general. Furthermore, an additional electric field (due to special-relativistic effects) contributes to the cross-field force balance in our case. This new piece of physics permits us to have asymptotically cylindrical solutions.

Finally, we write down the total power output enclosed within some flux surface $\psi_{\rm out}$

$$L = \int_0^{\psi_{\rm out}} k(\psi)\mu c^2\, d\psi\ , \tag{4.1}$$

where $k(\psi)$ is the mass flux per unit magnetic flux, which has the scaling $\psi^{1-2\beta}$. For a rough estimate, we shall take μ in equation (4.1) to be $2\,\sigma$ (see § 3.3). Since μ is independent of ψ and $\beta < 1$, the above integral is dominated by the outer flux surfaces, except in the limit of $\beta \to 1$ where all flux surfaces contribute equally to the power output. Making use of the definition of σ (cf. eq. [2.14b]), we have $L \cong \psi_{\rm out}^2 \Omega_{\rm out}^2/[4\pi(1-\beta)c]$, that is, the total power output enclosed within a flux surface is proportional to the square of the product of the angular momentum on that surface and the magnetic flux it encloses.

To summarize, our study of self-similar, relativistic winds has yielded the following results:

1. We demonstrate the existence of complete current-carrying, magnetized jet solutions. These results support the conclusions of our previous work on the collimation of relativistic MHD winds (Chiueh et al. 1991), which dealt only with asymptotically far-field solution.

2. For these collimated relativistic jets, the conversion of electromagnetic energy into plasma kinetic energy is much more efficient than for radial winds. We find that the final kinetic energy flux is comparable to the Poynting flux in general.

We thank Ellen Zweibel for useful conversations. This research was partially supported by National Science Foundation grants AST88-16140 and ATM85-06632, NASA Astrophysical Theory Center grant NAGW-766, the Alfred P. Sloan Foundation, and the National Science Council of Taiwan grant NSC79-0208-M008-32.

APPENDIX

The self-similar cross-field force balance equation (2.23) can be rewritten in the form of equation (2.36) when we use $t = \ln y$ as independent variable, where the denominator and the numerator in the square bracket of equation (2.36) are given by

$$D(t, x, x', \tau) = \dot{y}G(x, y, \dot{y}, \tau) = \frac{x}{1+\dot{y}^{-2}}\left\{\frac{1}{m_f^2}\left[\dot{y}^{-2} + \left(\frac{x\dot{y}^{-2}+x'}{x-x'}\right)^2\right] - \dot{y}^{-2}\right\}\left(\frac{1}{m_{\rm A}^2} - 1\right) \tag{A1}$$

and

$$\begin{aligned} N(t, x, x', \tau) = H(x, y, \dot{y}, \tau) = {} & \frac{x\dot{y}^{-2}+x'}{x-x'}\left\{\left(2-\frac{1}{\beta}\right)\frac{x(1+\dot{y}^{-2})}{x\dot{y}^{-2}+x'}\frac{1}{m_f^2}\left(\frac{1}{m_f^2}-1\right)\right. \\ & -\frac{1}{m_f^2}\left(\frac{1}{m_{\rm A}^2}-1\right) - \frac{\Gamma}{\tau}\left(\frac{1}{m_f^2}-1\right) + \frac{2\Gamma}{\tau^2}\left(1-\frac{1}{x_{\rm A}^2\eta}\right) + \frac{\Gamma^2}{\tau^3 x^2}\left(1-\frac{1}{\eta}\right)^2\Bigg\} \\ & + \frac{1}{\tau}\left(\frac{1}{m_f^2}-1\right)\left\{2 - \frac{x(1+\dot{y}^{-2})}{x-x'} + \left[\frac{1}{\tau x^2}\left(1-\frac{1}{\eta}\right)^2 - 1\right]\Gamma\right\}, \end{aligned} \tag{A2}$$

where Γ, $m_{\rm A}$, and m_f are defined in the text (eqs. [2.26] and [2.27]), and are not dependent on t explicitly. In fact, t comes into equation (2.36) explicitly only through

$$\dot{y}^{-2} = \left(\frac{dx}{dy}\right)^2 = \left(\frac{x'}{y}\right)^2 = (x'e^{-t})^2\ .$$

In general, near an asymptotically cylindrical surface of finite radius, one should have $t \to \infty$, $x' \to 0$, and $\tau \to \tau_\infty$, as $x \to x_\infty$. In this limit, $\dot{y}^{-2} \ll x' \ll 1$, and thus $D(t, x, x', \tau)$ and $N(t, x, x', \tau)$ approach the forms of equation (2.37), with the asymptotic constants

$D_1(x_\infty, \tau_\infty)$ and $N_0(x_\infty, \tau_\infty)$ given by

$$D_1(x, \tau) = \frac{1}{x m_f^2}\left(\frac{1}{m_A^2} - 1\right) \tag{A3}$$

and

$$N_0(x, \tau) = \frac{1}{\tau}\left(\frac{1}{m_f^2} - 1\right)\left\{\left(2 - \frac{1}{\beta}\right)\frac{\tau}{m_f^2} + 1 - \left[\frac{1}{\tau x^2}\left(1 - \frac{1}{\eta}\right)^2 - 1\right]\Gamma\right\}, \tag{A4}$$

where all quantities are to be evaluated at the limiting cylinder x_∞.

REFERENCES

Begelman, M. C., Blandford, R. D., & Rees, M. J. 1984, Rev. Mod. Phys., 56, 265
Blandford, R. D., & Payne, D. G. 1982, MNRAS, 199, 88 (BP)
Camenzind, M. 1986, A&A, 162, 32
———. 1987, A&A, 184, 341
———. 1989, in Accretion Disks and Magnetic Fields in Astrophysics, ed. G. Belvedere (Dordrecht: Kluwer), 129
Chiueh, T., Li, Z.-Y., & Begelman, M. C. 1991, ApJ, 377, 462
Goldreich, P., & Julian, W. H. 1970, ApJ, 160, 971
Heyvaerts, J., & Norman, C. A. 1989, ApJ, 347, 1055
Kennel, C. F., Fujimura, F. S., & Okamoto, I. 1983, Geophys. Astrophys. Fluid Dyn., 26, 147
Li, Z.-Y., & Begelman, M. C. 1992, in preparation
Lovelace, R. V. E., Mehanian, C., Mobarry, C. M., & Sulkanen, M. E. 1986, ApJS, 62, 1
Michel, F. C. 1969, ApJ, 158, 727
Okamoto, I. 1978, MNRAS, 185, 69
Phinney, E. S. 1983, Ph.D. thesis, University of Cambridge
Sakurai, T. 1985, A&A, 152, 121
———. 1987, PASJ, 39, 821
Sulkanen, M. E., & Lovelace, R. V. E. 1990, ApJ, 350, 732
Weber, E. J., & Davis, L., Jr. 1967, ApJ, 148, 217